



A Journal of the Gesellschaft Deutscher Chemiker

Angewandte Chemie

GDCh

International Edition

www.angewandte.org

Accepted Article

Title: A Light-up Logic Platform for Selective Recognition of Parallel G-Quadruplex Structures via Disaggregation-Induced Emission

Authors: Marco Deiana, Karam Chand, Jan Jamroskovic, Ikenna Obi, Erik Chorell, and Nasim Sabouri

This manuscript has been accepted after peer review and appears as an Accepted Article online prior to editing, proofing, and formal publication of the final Version of Record (VoR). This work is currently citable by using the Digital Object Identifier (DOI) given below. The VoR will be published online in Early View as soon as possible and may be different to this Accepted Article as a result of editing. Readers should obtain the VoR from the journal website shown below when it is published to ensure accuracy of information. The authors are responsible for the content of this Accepted Article.

To be cited as: *Angew. Chem. Int. Ed.* 10.1002/anie.201912027
Angew. Chem. 10.1002/ange.201912027

Link to VoR: <http://dx.doi.org/10.1002/anie.201912027>
<http://dx.doi.org/10.1002/ange.201912027>

RESEARCH ARTICLE

A Light-up Logic Platform for Selective Recognition of Parallel G-Quadruplex Structures via Disaggregation-Induced Emission

Marco Deiana^[a], Karam Chand^[b], Jan Jamroskovic^[a], Ikenna Obi^[a], Erik Chorell^{*[b]}, and Nasim Sabouri^{*[a]}

Abstract: The design of turn-on dyes with optical signals sensitive to the formation of supramolecular structures provides fascinating and underexplored opportunities for G-quadruplex (G4) DNA detection and characterization. Here, we show a new switching mechanism that relies on the recognition-driven disaggregation (on-signal) of an ultrabright coumarin-quinazoline conjugate. The synthesized probe selectively lights-up parallel G4 DNA structures via the disassembly of its supramolecular state, demonstrating outputs that are easily integrable into a label-free molecular logic system. Finally, our molecule preferentially stains the G4-rich nucleoli of cancer cells.

Introduction

Inspired by the complexity and hierarchical organization of natural occurring systems, chemists have constructed a multitude of artificial functional materials capable of completing sophisticated tasks at a molecular scale.^[1] As a result, a vast variety of mono-, bi- or tridimensional macro- and supramolecular homo- and heterostructures have been developed in recent years by exploiting the cooperativity between monomeric units.^[2] The tunable photophysical properties of organic dyes with donor- π -acceptor scaffolds and hydrogen-bonded/ π -surface-based intermolecular interaction sites have made them particularly attractive building-blocks for the construction of multistate nanostructures.^[3] Among those, coumarin-based compounds are considered archetypical dyes with a unique combination of both valuable optical properties and biological compatibility along with the tendency to form well-defined supramolecular architectures.^[4] However, in many conventional systems, the typical co-facial π -stacking arrangements of self-assembled luminophores, even at sub-micromolar concentrations, results in a partial or complete suppression of the emissive properties via relaxation of the excited-states through non-radiative channels (aggregation-caused quenching, ACQ).^[4a,5] From the viewpoint of real-life applications, this process hampers the widespread applicability of these types of optical probes and sensors, especially in the bio-sensing arena. In contrast, we hypothesized that these properties instead could be advantageous when utilized in the reversed way, i.e. through disaggregation-induced emission (DIE). This should

enable the use of this class of compounds in high-resolution and ultrasensitive spectroscopy and microscopy techniques. However, DIE still remains a poorly established and explored molecular recognition concept.^[6] Herein, we have extended DIE towards the detection of four-stranded G4 DNA structures, which have multiple regulatory biological functions and are recognized as novel therapeutic targets in e.g. oncology.^[7] To achieve this, we have coupled the coumarin scaffold with a quinazoline moiety to afford a more extended heterocyclic donor- π -acceptor scaffold with ability for self-assembly and G4 binding (Figure 1). One of the coumarin-quinazoline (CQ) conjugates proved to be capable of specific detection of parallel over non-parallel and non-G4 topologies. This derivative displayed striking optical changes upon binding the G4 scaffold, which enabled the construction of a label-free binary INHIBIT gate that may serve as a proof-of-principle for the future design of multifunctional molecular logic circuits. Furthermore, fluorescence imaging of fixed HeLa cells showed the ability of this compound to preferentially light-up the nucleoli which accommodate the multi-copy G4-rich ribosomal genes. Finally, mitochondria staining was observed in living cells which contain ~ 200 predicted G4 structures per mitochondrial DNA copy.^[8] Thus, this compound has light-up recognition properties for G4 DNA both *in vitro* and in cells.

Results and Discussion

Design, synthesis and self-assembly behavior

To identify compounds that signal the presence of a certain G4 DNA topology through DIE, we designed and synthesized a small set of CQ (1-6) derivatives (Figure 1).

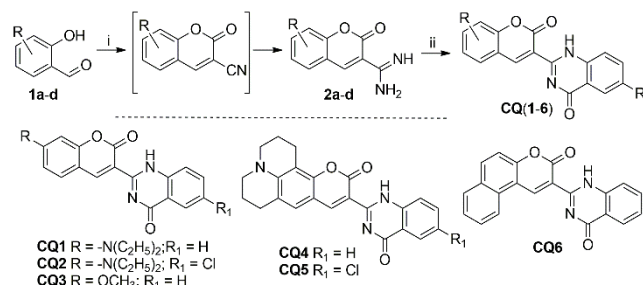


Figure 1. Synthetic route of coumarin-quinazoline (CQ) derivatives. Reagents and conditions: (i) Ammonium acetate, Ethyl cyanoacetate, absolute ethanol 15min, reflux, (76-81%); (ii) Isatoic anhydrides, *N,N*-Diisopropylethylamine, DMF, 100 °C, 12h (71-77%).

In the first step, Knoevenagel condensation of commercially available substituted ortho- hydroxyl benzaldehydes (1a-d) with ethyl cyanoacetate in presence of ammonium acetate led to *in*-

[a] Dr. M. Deiana, Dr. J. Jamroskovic, Dr. I. Obi, Dr. N. Sabouri
Department of Medical Biochemistry and Biophysics, Umeå
University, 90187 Umeå, Sweden
E-mail: nasim.sabouri@umu.se

[b] Dr. K. Chand, Dr. E. Chorell
Department of Chemistry, Umeå University, 90187 Umeå, Sweden
E-mail: erik.chorell@umu.se

Supporting information for this article is given via a link at the end of the document.

RESEARCH ARTICLE

situ formation of 3-cynocoumarin, which on subsequent reduction with another equivalent of ammonium acetate led to formation of the desired 3-amidinocoumarin intermediates (**2a-d**). In the second step, the 3-amidinocoumarin derivatives were reacted with different isatoic anhydrides under basic conditions to give the desired **CQ** (**1-6**) derivatives in 63-71% yields. The electron donating group in position 7 was varied with the aim to tune the fluorescence properties e.g. by a methoxy group (**CQ3**), a julolidine group (**CQ4** and **CQ5**) or a diethyl-amino group (**CQ1** and **CQ2**), the latter of which is prone to form nonradiative twisted intramolecular charge transfer (TICT) states. Additionally, derivatives with electron withdrawing groups were also synthesized to enhance the dipolar character of the molecules (**CQ2** and **CQ5**) as well as one derivative with an extended aromatic backbone (**CQ6**). Photophysical evaluation of all compounds showed that **CQ4** displayed suitable photostability and solubility properties compared to its analogues and was thus used for further in-depth DIE analysis.

Solvent dependence studies on the emission of **CQ4** displayed a moderate positive solvatochromic behavior (Figures S1-S3) and further analysis in aqueous buffered solution showed a very broad absorption band with maximum (λ_{max}) centered at 472 nm and an apparent extinction coefficient $\epsilon_{app} = 2.6 \times 10^4 \text{ M}^{-1} \text{ cm}^{-1}$ (Figure 2A, blue line), suggesting the formation of aggregated **CQ4** molecules. Indeed, atomic force microscopy (AFM) revealed the presence of small particles with average diameter of $\sim 33 \text{ nm}$ and a height of $\sim 3.9 \text{ nm}$ (Figure 2B). To probe if the addition of surfactants could disassemble **CQ4**, we carried out titrations with sodium dodecyl sulfate (SDS). At low concentrations, the surfactant affected the molecular aggregates weakly (Figure 2C). However, above the critical concentration of $0.75 \times 10^{-3} \text{ M}$, SDS induced a marked breakup of **CQ4** aggregates as determined by UV/Vis spectroscopy (Figure 2C). This process led to the formation of a new absorption band centered at 490 nm (Figure 2A, red line), which was ascribed to the monomer because of the overlap with the associated **CQ4** excitation spectrum (Figure S4), and the concomitant appearance of isosbestic points at 430 and 510 nm (Figure 2A). The strongly blue-shifted absorption maximum of **CQ4** in the absence of SDS is a clear evidence for an H-type exciton coupling between co-facial or "side-by-side" aggregated molecules.^[9] However, in addition to the band centered at 490 nm, the presence of SDS caused the formation of a new transition band centered at 526 nm, indicating the formation of slipped-stack packing arrangements with the "head-to-tail" J-type coupling (Figure 2A).^[9] It is important to note that the gradual addition of SDS induced the concomitant disappearance of the J-aggregates along with the formation of the monomeric state with $\epsilon_{app} = 5.4 \times 10^4 \text{ M}^{-1} \text{ cm}^{-1}$ (Figure 2C). Concentration-dependent UV/Vis experiments provided the aggregation constant ($K_{agg} = 8.1 \times 10^5 \text{ M}^{-1}$) (Figure S5). To further examine the molecular aggregates, we performed steady-state fluorescence measurements before and after the addition of SDS (Figure 2D). In the absence of the surfactant, the **CQ4** emission intensity was remarkably quenched supporting the formation of new competitive radiationless relaxation pathways that are available in the co-facial aggregated states. On the other hand, in

the presence of SDS **CQ4** underwent gradual disassembly and exhibited intense photoluminescence. Similar changes in fluorescence were also observed upon decreasing the water volume fraction $\chi_{(water)}$ in a MeOH/water mixture (Figure S6), suggesting that photoluminescence is enhanced when the **CQ4** aggregates are disassembled in MeOH.

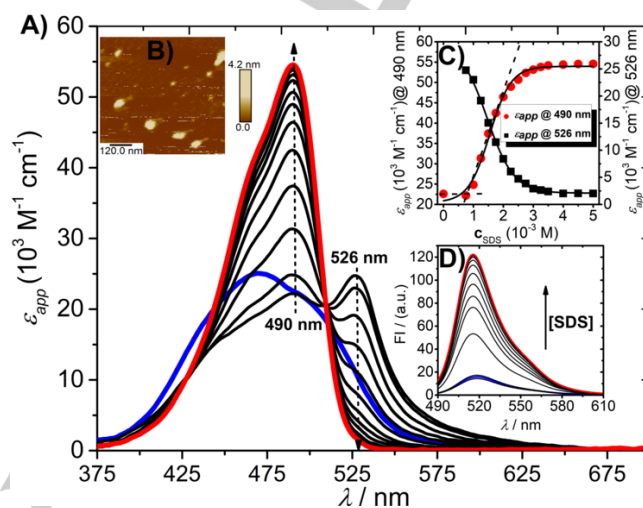


Figure 2. A) UV/Vis absorption spectral changes of a buffered aqueous **CQ4** solution ($c_{CQ4} = 3.8 \mu\text{M}$, Tris buffer $c = 50 \text{ mM}$, $\text{pH} = 7.5$) before (blue line) and after the gradual addition of SDS from 0 to 5 mM (red line). B) AFM height image on mica of a **CQ4** aqueous solution ($c_{CQ4} = 10 \mu\text{M}$). C) Evolution of the absorption profile of **CQ4** in the presence of SDS. Black lines correspond to a fitting with a growth sigmoidal Boltzmann function. The dashed black lines aim to show the critical concentration of $0.75 \times 10^{-3} \text{ M}$. D) **CQ4** emission profile in the presence of different concentrations of SDS.

G4-CQ4 interactive binding models

In a similar fashion to the SDS-induced disaggregation, we speculated that binding of **CQ4** to the planar π -surfaces of G4 DNA structures may also cause the disassembly of the molecular aggregates into highly emissive monomeric states. We thus studied the recognition process of **CQ4** towards a large panel of biologically relevant synthetic and natural G4 DNA structures with various topologies including parallel, hybrid, and antiparallel G4s (see Table S1 and Figures S7-S9, S10-S35). Indeed, G4 DNA successfully disassembled **CQ4** aggregates and this effect was strongly pronounced for parallel G4 structures (Figures 3, 4 and Table 1). The proposed interactive binding model between **CQ4** and G4 and non-G4 structures is shown in Figure 3.

The association constant (K_a) values of **CQ4** complexed with parallel G4 DNA structures were up to three-orders of magnitude (i.e. ≥ 1000 -fold) higher compared to those calculated in the presence of non-parallel G4 structures (Figure 4A and Table 1). This outcome can be rationalized by the highly accessible hydrophobic external G-tetrads in parallel G4 architectures.^[6b]

RESEARCH ARTICLE

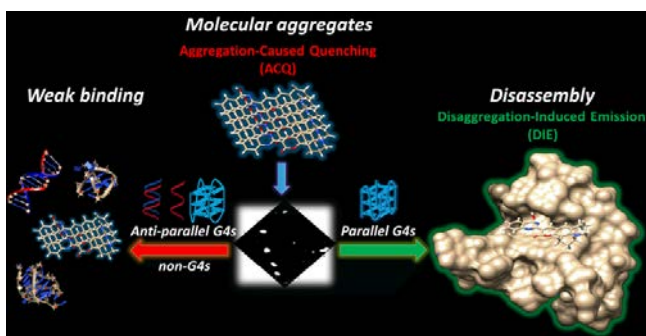


Figure 3. Schematic illustration of the selective detection mechanism: **CQ4** forms molecular aggregates in solution with ACQ signatures (middle). In the presence of parallel G4s, the formation of stable complexes turns the weakly emissive aggregated states into highly emissive G4-**CQ4** monomeric adducts through a DIE process (right panel). Conversely, antiparallel and non-G4 structures are unable to fully displace the aggregated state of **CQ4** resulting in a poor fluorescence recovery (left panel).

Importantly, within the same experimental conditions, no binding was observed for **CQ4** in the presence of long genomic double-stranded DNA (ds-DNA), and the light-up response of **CQ4** was hardly affected by the presence of 50 equivalents excess of competitive ds-DNA (Figure S36). Parallel G4 over duplex selectivity can be explained by the difference between their respective binding surfaces where G4 presents a larger and more accessible surface area for π -stacking compared to duplex DNA.^[7c]

To further evaluate the selectivity of **CQ4** for parallel G4 structures, non-denaturing polyacrylamide gel electrophoresis (PAGE) were performed. These gels were loaded with the folded G4 and non-G4 oligonucleotides, post-stained with **CQ4**, and imaged. These images confirmed the outstanding selectivity of the probe for parallel G4 topologies (Figures 4B and S37). It is worth to keep in mind that according to previous published papers most of the parallel G4 structures studied here yielded heterogeneous solutions with multiple G4 forms (e.g. intra and intermolecular folding).^[10]

The strongest DIE effect was observed in the presence of *c-MYC* sG4. This G4 structure lacks the terminal flanking sequences at both 5'- and 3'-ends (compare *c-MYC* sG4 vs. *c-MYC* Pu22) and thus provides better π -stacking possibilities for the planar conformation of the π -extended **CQ4** core, which can explain the more efficient disaggregation process. To study this in more detail, the UV/Vis spectral changes were analyzed when **CQ4** was complexed with *c-MYC* sG4 (Figure 5). This resulted in the narrowing of the absorption band (isosbestic points at 463 and 512 nm) along with the formation of a new red-shifted transition band centered at 494 nm (Figure 5). The fluorescence emission intensity of **CQ4** was partially quenched in its unbound state (photoluminescence quantum yield (PLQY), $\Phi_{F(CQ4)} = 0.42 \pm 0.01$). However, the addition of *c-MYC* sG4 greatly increased the fluorescence response of **CQ4** providing near-unity PLQY ($\Phi_{F(CQ4:c-MYC\ sG4)} = 0.95 \pm 0.2$), one of the highest values reported so far for G4-binders (Figure 5 and Table 1).^[11] This result clearly supports the formation of a *c-MYC* sG4-**CQ4** complex via the direct interaction of the **CQ** π -surfaces with the hydrophobic G-tetrad core of the *c-MYC* sG4 DNA structure. It is important to

note, that the linear response of the fluorescence intensity of **CQ4** as a function of *c-MYC* sG4 concentration provided a limit of detection (LOD) of 83.5 ± 4.2 nM awarding this probe as one of the most sensitive parallel G4-binders reported so far (Figure 5,

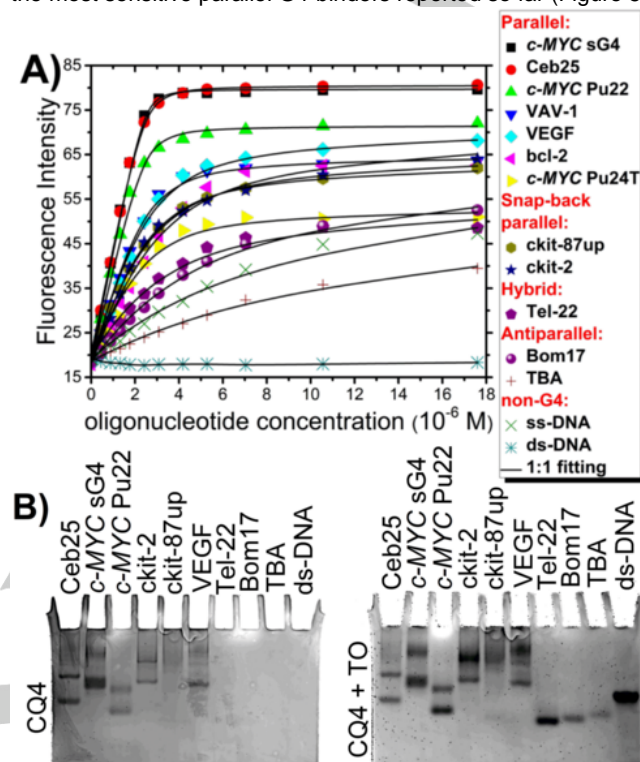


Figure 4. A) Fluorescence titration of **CQ4** in the presence of a large panel of G4 and non-G4 structures shows a clear-cut preference for parallel G4 topologies. The solid black lines correspond to a 1:1 fitting model at λ_{em} . **B)** Non-denaturing PAGE images of G4 and non-G4 structures stained with **CQ4** (left-panel). The same gel was also co-stained with thiazole orange TO, (right panel) to show the specificity of binding. $c_{CQ4} = 1 \mu M$, $c_{TO} = 5 \mu M$ and $C_{oligos} = 10 \mu M$, $\lambda_{exc} = 488$ nm.

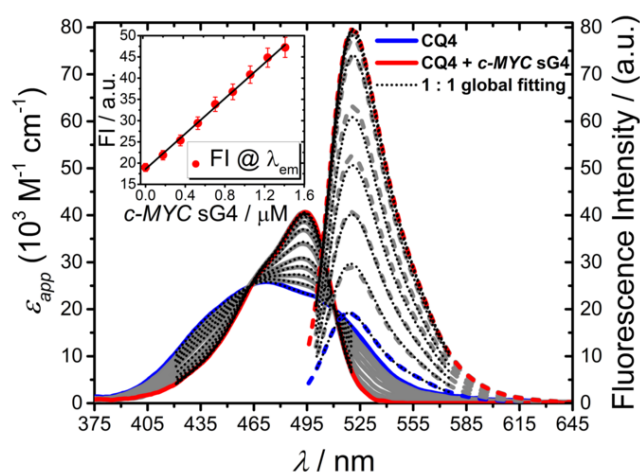


Figure 5. UV/Vis absorption (solid lines) and fluorescence emission spectra (dashed lines) of **CQ4** upon gradual addition of *c-MYC* sG4 ($c_{CQ4} = 3.8$ or $2.5 \mu M$, Tris buffer $c = 50$ mM, KCl = 100 mM, pH = 7.5). Superimposed dotted lines

RESEARCH ARTICLE

correspond to a 1:1 global fitting model. Inset, calculated limit of detection (LOD) for **CQ4**-*c*-MYC sG4 system.

inset).^[6b,6d] Moreover, the optical changes arising in the absorption and emission profiles resulted in excellent one-photon brightness (defined as the product of $\epsilon_{max} \times \Phi_F$) of $3.9 \times 10^4 \text{ M}^{-1} \text{ cm}^{-1}$.

Ionic strength-dependence studies showed that *c*-MYC sG4 was more stable under K^+ conditions compared to Na^+ or Li^+ conditions, which is fully consistent with the ability of **CQ4** to strongly light-up the *c*-MYC sG4 sequence stabilized by K^+ ions (Figures S38-S40).

To further examine the steady-state emission data, the photophysical properties of the **CQ4** excited state was investigated via time-correlated single photon counting (TCSPC) measurements (Figure S41). The decay traces of the free and bound **CQ4** molecules were fitted with a biexponential function (Table S2). In its free form, **CQ4** exhibited an average time-dependent decay of 3.38 ns, which was increased to 4.76 ns in the presence of *c*-MYC sG4. In line with previous results, this suggest that parallel G4 DNA structures are able to disassemble the aggregated **CQ4** and induce additional geometrical (vibrational and rotational) and/or structural (molecular conformation) restrictions of **CQ4** in the G4:**CQ4** complex. This was further supported by the inhibition of the nonradiative relaxation pathways ($k_{nr(\text{CQ4})} = 1.73 \times 10^8 \text{ s}^{-1}$ vs. $k_{nr(\text{CQ4}:\text{c-MYC sG4})} = 1.11 \times 10^7 \text{ s}^{-1}$) and increase of the radiative channels ($k_{r(\text{CQ4})} = 1.23 \times 10^8 \text{ s}^{-1}$ vs. $k_{r(\text{CQ4}:\text{c-MYC sG4})} = 1.99 \times 10^8 \text{ s}^{-1}$) in the G4:**CQ4** complex.

Next, the binding stoichiometry of the complex in solution was assessed using the mole ratio and Job's plot methods. We found a clear-cut preference for 1:1 **CQ4**:*c*-MYC sG4 stoichiometry (Figures 6, S42 and S43).

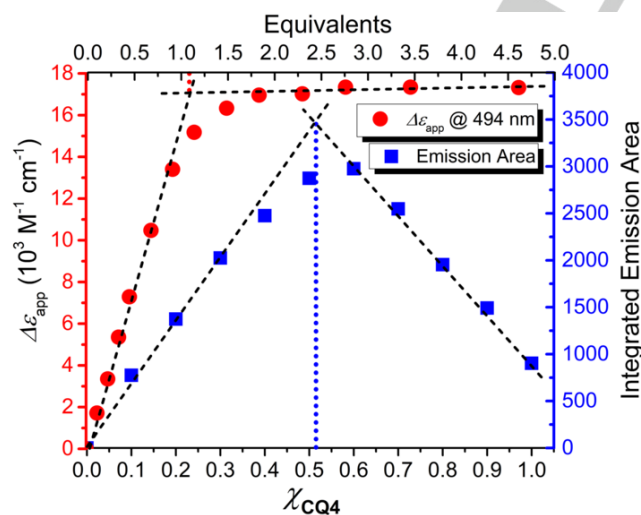
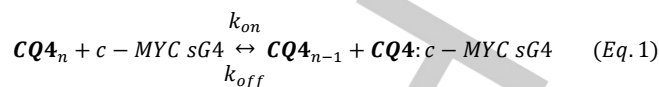


Figure 6. Mole ratio and Job's plot methods for assessing the **CQ4**:*c*-MYC sG4 stoichiometry. The vertical dotted lines aim to show the stoichiometry of the system.

A quantitative binding analysis using global fitting on both the absorption and emission data provided the association constant (K_a) = $3.5 \times 10^7 \text{ M}^{-1}$ (Table 1).

The mechanism of interaction of **CQ4** with *c*-MYC sG4 was investigated by using the following dissociation model:^[12]



where **CQ4**_n, *c*-MYC sG4 and **CQ4**:*c*-MYC sG4 represent the **CQ4** aggregate, the G4 structure and the complex of **CQ4** with *c*-MYC sG4, respectively. Such a model would predict an increase in the apparent rate constant of dissociation of the **CQ4** aggregate with an increase in concentration of *c*-MYC sG4. As shown in Figure 7 the apparent rate constant increased with increasing *c*-MYC sG4 concentration indicating that the G4 structure binds and catalyzes dissociation of **CQ4** molecular aggregates.^[12]

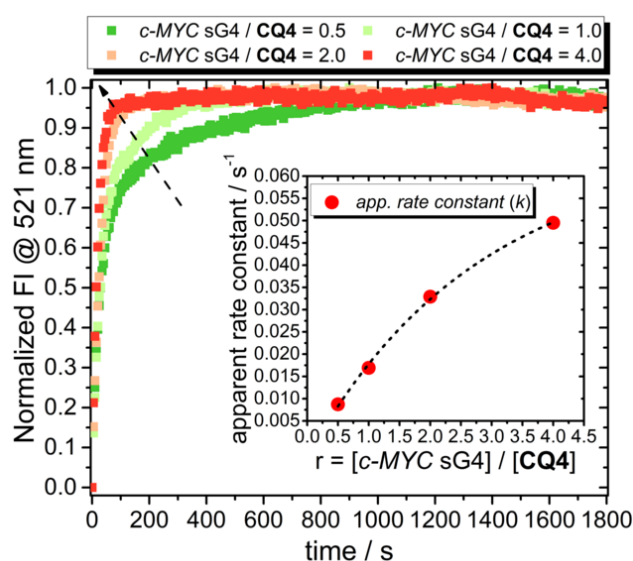


Figure 7. Effect of increasing concentration of *c*-MYC sG4 on the dissociation kinetics of **CQ4** aggregates. Apparent rate constant (k) was obtained by fitting the kinetic data to a monoexponential function.

Table 1. Summary of the spectroscopic properties and binding constants of **CQ4** complexed with G4 and non-G4 DNA structures.

DNA	λ_{max} nm	$\epsilon_{max} \times 10^3 \text{ M}^{-1} \text{ cm}^{-1}$	λ_{em} nm	$K_a \text{ M}^{-1[a]}$	$\Phi_F^{[b]}$	τ / ns	Str ^[d]
<i>c</i> -MYC sG4	494	40.6	521	3.5×10^7	0.95	4.76	P
Ceb25	495	38.2	519	1.7×10^7	0.97	4.55	P
<i>c</i> -MYC Pu22	496	34.5	520	1.4×10^7	0.91	—	P
VAV-1	495	36.6	521	2.0×10^6	0.91	4.57	P
VEGF	494	34.2	521	1.2×10^6	0.88	4.36	P
bcl-2	495	32.7	520	5.1×10^5	—	4.54	P
<i>c</i> -MYC Pu24T	496	29.1	519	1.0×10^6	—	—	P
ckit-87up	496	33.4	520	1.1×10^6	—	—	P ^{sb}
ckit-2	496	34.7	519	1.4×10^6	—	—	P ^{sb}
Tel-22	492	28.7	516	3.5×10^5	—	—	H

RESEARCH ARTICLE

Bom17	491	21.6	517	2.6×10^4	—	—	AP
TBA	492	22.1	519	2.0×10^5	—	—	AP
ss-DNA	495	28.0	519	2.3×10^5	—	—	nG4
ds-DNA	474	18.0	519	—	—	$3.53^{[c]}$	nG4

[a] Data fitting with 1:1 binding model was obtained with Bindfit by using multiple global fitting methods (Nelder-Mead method).^[13] The association constants are evaluated by using the average values of both spectrophotometric and fluorimetric titrations. [b] Fluorescein is used as reference standard (0.1 M NaOH, $\Phi_F = 0.95$). [c] ds-DNA was used with an excess of 50 eq. than respect to the **CQ4** concentration. [d] Str = topological structure, P = parallel, P^{sb} = snap-back parallel, H = hybrid, AP = antiparallel and nG4 = non-G4 structure.

Next, by performing electronic circular dichroism (ECD) spectroscopy we assessed the morphological changes occurring on the *c-MYC* sG4 structure in the presence of **CQ4** (Figures S44 and S45). The ECD spectra showed that the overall secondary structure of *c-MYC* sG4 was fully conserved even upon the addition of an excess of 4 eq. of ligand.^[6b,6c] Therefore, in spite of the high K_a value determined, **CQ4** does not induce any topological changes or destabilization effect on the G4 scaffold, a highly important feature in the design of ideal *in vivo* G4 fluorescent probes.

This statement was further investigated by using the DNA polymerase stop assay for G4-interactive small molecules.^[14] If **CQ4** stabilizes the G4 structure, and thereby enhances the pausing/ arrest of the DNA polymerase on the G4 DNA template, the position and amount of pausing as well as the amount of full-length product can be detected and quantified on a denaturing polyacrylamide gel. **CQ4** did not increase DNA replication stalling, suggesting that **CQ4** does not stabilize the G4 structures (Figure S46). The lack of any well-resolved induced circular dichroism (ICD) signals corroborates the current hypothesis of a π -stacking binding mode. Concentration-dependent **CQ4**-fluorescence signal displacement by the well-known G4 end-stacker Phen-DC₃ confirmed the end-stacking ability of our probe (Figure 8).^[15] These results highlighted the strong competitive behavior of the two molecules for the same binding site.

Cellular imaging

Confocal laser scanning microscopy (CLSM) was used to evaluate **CQ4** cellular emission fingerprint. Fixed HeLa cells treated with **CQ4** revealed intense green fluorescence signals in the nuclear and cytoplasmic/mitochondrial regions with clear peaks in the subnuclear compartments whose appearance was compatible with that of nucleoli (Figure 9A).^[16] Following the *in vitro* evidence of **CQ4**'s high selectivity for parallel DNA G4 structures, we treated cells with RNase to confirm the nature of the main binding target of the compound (Figure 9B, upper panel). Thioflavin-T (ThT) was used as control since it is also intracellularly fluorescent and known to bind RNA G4s making it highly sensitive to RNase treatment (Figure 9B, lower panel).^[17] While RNase treatment did not modify **CQ4** nucleolar staining, the nucleolar ThT signal was reduced by the presence of the enzyme,

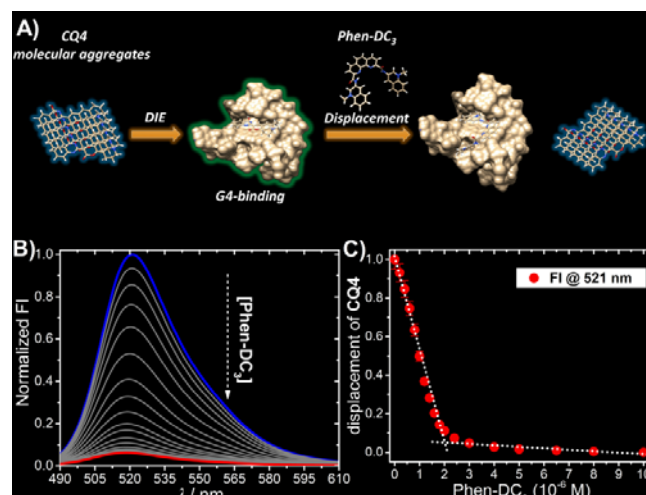


Figure 8. A) Schematic illustration of the fluorescence displacement assay performed by using the G4 end-stacker Phen-DC₃. B-C) Fluorescence emission changes on the **CQ4**-*c-MYC* sG4 system upon increasing concentration of Phen-DC₃ (**CQ4** = 2 μ M, *c-MYC* sG4 = 2 μ M and Phen-DC₃ ranged from 0 to 10 μ M).

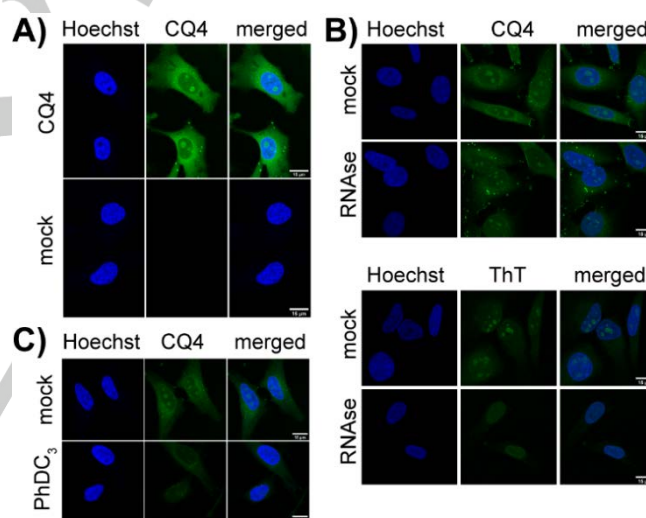


Figure 9. A) Confocal fluorescence images of fixed HeLa cells stained with **CQ4** (1 μ M) and Hoechst 33342. B) Fluorescence images of HeLa cells stained with Hoechst and **CQ4** (1 μ M) before and after treatment with RNase (upper panel). Fluorescence images of Hoechst and ThT (1 μ M) before and after treatment with RNase (lower panel). C) Fluorescence displacement assay between **CQ4** (1 μ M) and Phen-DC₃ (5 μ M). Scale bar = 15 μ m. In Figures A and C, Diode 405 nm laser was used for Hoechst $\lambda_{exc} = 405$ nm, $\lambda_{em} = 415-450$ nm; WLL laser was used for **CQ4** visualization $\lambda_{exc} = 472$ nm, $\lambda_{em} = 482-794$ nm. Additional washing during Phen-DC₃ displacement in Figure 9C caused decrease in overall **CQ4** signal intensity. In Figure B, Diode 405 nm laser was used for Hoechst $\lambda_{exc} = 405$ nm, $\lambda_{em} = 415-430$ nm; for ThT visualization Argon laser $\lambda_{exc} = 458$ nm, $\lambda_{em} = 468-782$ was used; for **CQ4** Argon laser $\lambda_{exc} = 476$ nm, $\lambda_{em} = 486-782$ was used.

indicating the ability of **CQ4** to preferentially target DNA G4 structures. DNase treatment was not performed due to the apparent inability of this enzyme to reach the nucleoli.^[16c] Instead, DNA G4 binding was confirmed by using the well-known G4-

RESEARCH ARTICLE

binder Phen-DC₃ (Figures 9C and S47). Indeed, Phen-DC₃ completely displaced **CQ4** from the subnuclear G-rich compartment even at low concentration. Finally, CLSM imaging of living HeLa cells showed co-localization of **CQ4** with Mitotracker, suggesting that **CQ4** co-localize with the mitochondrial network (Figure S48). Mitochondrial targeting has recently gained considerable attention being a potential target for cancer treatment with hundreds of possible G4 forming sequences at the DNA level, with many forming parallel G4 structures.^[8]

Logic-gate

Although DNA have been used to construct various logic platforms, the inability to generate detectable signals has forced the development of DNA-based circuits that rely on suitable optical reporters.^[18] In this context, multitasking supramolecular fluorescence sensors with distinguishable readout responses are key components in the ongoing quest towards increasingly sophisticated, sensitive, and versatile information processing systems. Therefore, as **CQ4** showed several assembly behaviors associated with different binding conditions, we further examined its applicability as a building-block for the construction of multi-output logic circuits. As proof-of-concept, we focused our attention on the INHIBIT gate, one of the most widely used Boolean gates in biochemical detections (Figure 10A). The threshold of the output signals was set at 0.3, and any signal greater than this value was defined as "1" whereas, those lower than the threshold signal value were defined as "0".

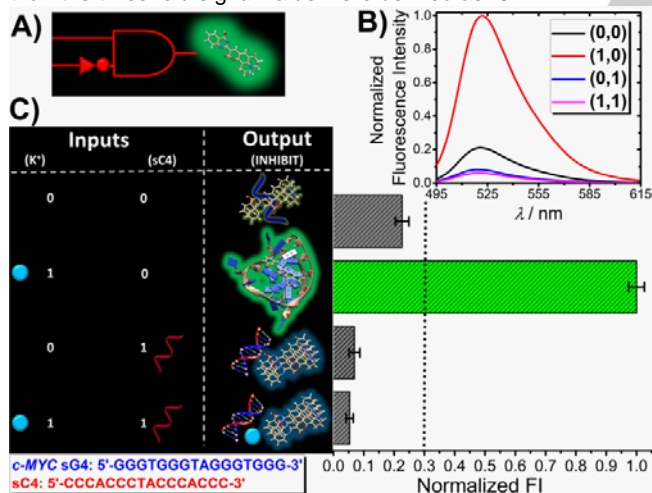


Figure 10. A) Diagram of the operational design of the binary INHIBIT gate. B) Fluorescence spectra of **CQ4** with different input conditions. C) Schematic truth table (left-panel) of the binary INHIBIT gate and associated normalized fluorescence responses plotted as a bar chart (right-panel). The dotted black line shows the threshold value (0.3). The blue single-stranded DNA sequence represents the G-rich oligonucleotide *c-MYC* sG4, the light-blue circle refers to K⁺ ions, the red single-stranded DNA sequence indicates the C-rich oligonucleotide sC4.

CQ4 together with the non-folded single-stranded *c-MYC* sG4 sequence were used as the initial state, whereas K⁺ and the complementary C-strand (hereafter referred as sC4) were used as the input stimuli. As depicted in Figures 10B and 10C, **CQ4**

showed a weak fluorescence signal in the presence of the non-folded single-stranded *c-MYC* sG4 sequence. However, upon addition of K⁺ that catalyze the folding of *c-MYC* sG4, **CQ4** strongly emitted a fluorescence signal. In contrast, the addition of the complementary strand, sC4, resulted in the formation of ds-DNA that could not disaggregate the **CQ4** templates thus inducing no or very weak fluorescence changes both in the absence or the presence of K⁺ ions. These results thus fully support the proper execution of an INHIBIT gate (Figure 10C).

Conclusion

In conclusion, a **CQ**-based dye, **CQ4**, was designed to display a supramolecular and solvatochromic feature. The possibility to use the striking optical changes of **CQ4** associated with multiple assembly states for DIE purposes was evaluated using a large panel of biologically relevant G4 structures. This revealed that the probe was able to selectively signal the presence of parallel G4 DNA topologies over both antiparallel and hybrid G4 DNA topologies as well as non-G4 DNA structures. Moreover, we applied the optical and supramolecular changes of our sensor in a tunable label-free DNA-based logic nanoplatform through the design of a binary INHIBIT gate. The presented recognition mechanism thus provides a promising and underexplored route to design selective and sensitive turn-on probes and advanced multi-output logic circuits. Finally, the ability of **CQ4** to target DNA G4 structures in human cells opens new avenues toward the design of potential sequence-selective *in vivo* supramolecular G4 fluorescent probes. A strategy that is currently under investigation in our laboratories.

Experimental Section

Experimental details, including materials and methods, experimental procedures, optical studies, G-quadruplex characterization, G-quadruplex binding studies, microscopy, and chemical synthesis of the compounds, are provided in the Supporting Information.

Acknowledgements

Work in the Sabouri lab was supported by Knut and Alice Wallenberg Foundation (KAW2015-0189) and the Swedish Research Council. MD was supported by a fellowship from the MIMS Excellence by Choice Postdoctoral Programme. Work in the Chorell lab was supported by the Kempe foundations (SMK-1632) and the Swedish Research Council. We thank Prof. Sjoerd Wanrooij for the kind gift of HeLa cells and Dr. Mara Doimo for her expert advice with microscopy. We acknowledge Dr. Igor lashchishyn for assistance with AFM imaging. We also acknowledge Dr. Irene Martinez Carrasco and the Biochemical Imaging Center at Umeå University and the National Microscopy Infrastructure (VR-RFI 2016-00968) for providing assistance in microscopy.

RESEARCH ARTICLE

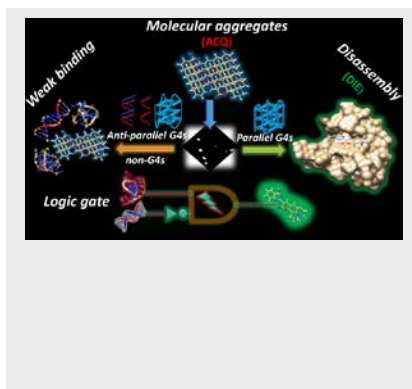
Keywords: aggregation • coumarin • DNA • G-quadruplex • logic gate

- [1] a) J. M. Abendroth, O. S. Bushuyev, P. S. Weiss, C. J. Barrett, *ACS Nano* **2015**, *9*, 7746-7768; b) S. Dhiman, A. Jain, M. Kumar, S. J. George, *J. Am. Chem. Soc.* **2017**, *139*, 16568-16575; c) V. Grande, B. Soberats, S. Herbst, V. Stepanenko, F. Würthner, *Chem. Sci.* **2018**, *9*, 6904-6911; d) Y. Kim, H. Li, Y. He, X. Chen, X. Ma, M. Lee, *Nat. Nanotechnol.* **2017**, *12*, 551-556; e) T. Tian, Y. Song, L. Wei, J. Wang, B. Fu, Z. He, X. -R. Yang, F. Wu, G. Xu, S. -M. Liu, C. Li, S. Wang, X. Zhou, *Nucleic Acid Res.* **2017**, *45*, 2283-2293; f) F. della Sala, S. Maiti, A. Bonanni, P. Scrimin, L. J. Prins, *Angew. Chem. Int. Ed.* **2018**, *57*, 1611-1615; g) A. Sarkar, S. Dhiman, A. Chalisehar, S. J. George, *Angew. Chem. Int. Ed.* **2017**, *56*, 13767-13771; h) S. Maiti, I. Fortunati, C. Ferrante, P. Scrimin, L. J. Prins, *Nat. Chem.* **2016**, *8*, 725-731.
- [2] a) D. Pijper, B. L. Feringa, *Soft Matter*, **2008**, *4*, 1349-1372; b) Y. Kamiya, H. Asanuma, *Acc. Chem. Res.* **2014**, *47*, 1663-1672.
- [3] a) T. Aida, E. W. Meijer, S. I. Stupp, *Science* **2012**, *335*, 813-817; b) F. Würthner, *Acc. Chem. Res.* **2016**, *49*, 868-876; c) S. Ghosh, V. K. Praveen, A. Ajoyghosh, *Annu. Rev. Mater. Res.* **2016**, *46*, 235-262.
- [4] a) F. Bu, R. Duan, Y. Xie, Y. Yi, Q. Peng, R. Hu, A. Qin, Z. Zhao, B. Z. Tang, *Angew. Chem. Int. Ed.* **2015**, *54*, 14492-14497; b) M. Tasiór, D. Kim, S. Singha, M. Krzeszewski, K. H. Ahn, D. T. Gryko, *J. Mater. Chem. C* **2015**, *3*, 1421-1446; c) X. Liu, J. M. Cole, K. S. Low, *J. Phys. Chem. C* **2013**, *117*, 14723-14730; d) X. Liu, J. M. Cole, P. C. Y. Chow, L. Zhang, Y. Tan, T. Zhao, *J. Phys. Chem. C* **2014**, *118*, 13042-13051; e) P. Verma, H. Pal, *J. Phys. Chem. A* **2012**, *116*, 4473-4484; f) L. G. Meimetis, J. C. T. Carlson, R. J. Giedt, R. H. Kohler, R. Weissleder, *Angew. Chem. Int. Ed.* **2014**, *53*, 7531-7534; g) C. Uttamapinant, K. A. White, H. Baruah, S. Thompson, M. Fernández-Suárez, S. Puthenveetil, A. Y. Ting, *Proc. Natl. Acad. Sci. USA* **2010**, *107*, 10914-10919; h) G. Signore, R. Nifosi, L. Albertazzi, B. Storti, R. Bizzarri, *J. Am. Chem. Soc.* **2010**, *132*, 1276-1288.
- [5] J. Mei, N. L. C. Leung, R. T. K. Kwok, J. W. Y. Lam, B. Z. Tang, *Chem. Rev.* **2015**, *15*, 11718-11940.
- [6] a) D. Zhai, W. Xu, L. Zhang, Y. -T. Chang, *Chem. Soc. Rev.* **2014**, *43*, 2402-2411; b) V. Grande, F. Doria, M. Freccero, F. Würthner, *Angew. Chem. Int. Ed.* **2017**, *56*, 7520-7524; c) V. Grande, C. -A. Shen, M. Deiana, M. Dudek, J. Olesiak-Banska, K. Matczyszyn, F. Würthner, *Chem. Sci.* **2018**, *9*, 8375-8381; d) M. Zuffo, A. Guédin, E. -D. Leriche, F. Doria, V. Pirota, V. Gabelica, J. -L. Mergny, M. Freccero, *Nucleic Acid Res.* **2018**, *46*, e115; e) L. Zhang, J. C. Er, K. K. Ghosh, W. J. Chung, J. Yoo, W. Xu, W. Zhao, A. T. Phan, Y. -T. Chang, *Sci. Rep.* **2014**, *4*, 3776.
- [7] a) R. Hänsel-Hertsch, M. Di Antonio and S. Balasubramanian, *Nat. Rev. Mol. Cell Biol.* **2017**, *18*, 279-284; b) S. Balasubramanian, L. H. Hurley, S. Neidle, *Nat. Rev. Drug Discov.* **2011**, *10*, 261-275; c) S. Neidle, *Nat. Rev. Chem.* **2017**, *1*, 0041.
- [8] A. Bedrat, L. Lacroix, J. -L. Mergny, *Nucleic Acid Res.* **2016**, *44*, 1746-1759.
- [9] F. Würthner, T. E. Kaiser, C. R. Saha-Möller, *Angew. Chem. Int. Ed.* **2011**, *50*, 3376-3410.
- [10] H. T. Le, M. C. Miller, R. Buscaglia, W. L. Dean, P. A. Holt, J. B. Chaires, J. O. Trent, *Org. Biomol. Chem.* **2012**, *10*, 9393-9404.
- [11] Y. V. Suseela, N. Narayanaswamy, S. Pratihari, T. Govindaraju, *Chem. Soc. Rev.* **2018**, *47*, 1098-1131.
- [12] V. G. Panse, P. Vogel, W. E. Trommer, R. Varadarajan, *J. Biol. Chem.* **2000**, *275*, 18698-18703.
- [13] a) P. Thordarson, *Chem. Soc. Rev.* **2011**, *40*, 1305-1323; b) L. K. S. von Krbek, C. A. Schalley, P. Thordarson, *Chem. Soc. Rev.* **2017**, *46*, 2622-2637.
- [14] H. Han, L. H. Hurley, M. Salazar, *Nucleic Acid Res.* **1999**, *27*, 537-542.
- [15] W. J. Chung, B. Heddi, F. Hamon, M. -P. Teulade-Fichou, A. T. Phan, *Angew. Chem. Int. Ed.* **2014**, *53*, 999-1002.
- [16] a) J. Li, X. Yin, B. Li, X. Li, Y. Pan, J. Li, Y. Guo, *Anal. Chem.* **2019**, *91*, 5354-5361; b) O. Domarco, C. Kieler, C. Pirker, C. Dinhof, B. Englinger, J. M. Reisecker, G. Timelthaler, M. D. Garcia, C. Peinador, B. K. Keppler, W. Berger, A. Terenzi, *Angew. Chem. Int. Ed.* **2019**, *58*, 8007-8012; c) F. Doria, M. Nadai, M. Zuffo, R. Perrone, M. Freccero, S. N. Richter, *Chem. Commun.* **2017**, *53*, 2268-2271.
- [17] S. Zhang, H. Sun, H. Chen, Q. Li, A. Guan, L. Wang, Y. Shi, S. Xu, M. Liu, Y. Tang, *Biochim. Biophys. Acta Gen. Subj.* **2018**, *1862*, 1101-1106.
- [18] a) H. -Z. He, D. S. -H. Chan, C. -H. Leung, D. -L. Ma, *Nucleic Acid Res.* **2013**, *41*, 4345-4359; b) C. Yang, S. Yang, J. Li, Y. Du, L. Song, D. Huang, J. Chen, Q. Zhou, Q. Yang, Y. Tang, *Anal. Chem.* **2018**, *90*, 10585-10590.

RESEARCH ARTICLE

RESEARCH ARTICLE

A versatile supramolecular sensing platform based on the switching mechanism of a self-aggregated coumarin-quinazoline derivative was used to selectively detect parallel G-quadruplex (G4s) DNA structures both *in vitro* and in cells. The programmed reorganization of tightly packed chromophores was further used to build up a programmable label-free molecular logic system.



Marco Deiana, Karam Chand, Jan Jamroskovic, Ikenna Obi, Erik Chorell*, Nasim Sabouri*

Page No. – Page No.

A Light-up Logic Platform for Selective Recognition of Parallel G-Quadruplex Structures via Disaggregation-Induced Emission

Accepted Manuscript